Early thermal and structural evolution of small bodies in the trans-Neptunian zone

Rainer Merk* and Dina Prialnik (dina@planet.tau.ac.il)
Department of Geophysics and Planetary Sciences
Sackler Faculty of Exact Sciences, Tel Aviv University, Ramat Aviv 69978, Israel

Abstract.
Early evolution of trans-Neptunian objects, commonly known as Kuiper Belt objects (KBOs), is the result of heating due to radioactive decay, the most important source being ^{26}Al. Several studies are reviewed, dealing with the long-term evolution of KBO models, calculated by means of 1-D numerical codes that solve the heat and mass balance equations on a fixed spherically symmetric grid. It is shown that, depending on parameters, the interior may reach quite high temperatures. The models thus suggest that KBOs are likely to lose the ices of very volatile species during early evolution; ices of less volatile species are retained in the cold subsurface layer. As the initially amorphous ice is shown to crystallize in the interior, some objects may also lose part of the volatiles trapped in amorphous ice. Generally, the outer layers are far less affected than the inner part, resulting in a stratified composition and altered porosity distribution.

It is further shown that the thermal evolution of KBOs cannot be treated separately from their accretional evolution, as the processes occur in parallel. A systematic attempt to calculate accretion and thermal evolution simultaneously is presented, based on a numerical moving grid scheme. The accretion rate is obtained from the solution of the coupled coagulation equations for gravitationally interacting planetesimals. The effect of planetesimal velocities on the accretion scheme is included by a simplified equipartition argument. The time dependent accretion rates serve as input for the numerical solution of the heat transport equation for growing bodies mainly heated by radioactive decay of ^{26}Al, allowing for phase transitions. Calculations carried out over the parameter space [heliocentric distance; final radius; ice fraction] lead to conclusions regarding the structure of KBOs, such as melt fraction, or extent of crystalline ice region.

Keywords: comets: general — comets: interiors — Kuiper Belt

1. Introduction – Can KBOs be altered by early evolution ?

Kuiper Belt objects bear resemblance both to asteroids and to comets. Like asteroids, they are found in a region of the solar nebula where they were originally formed. Comets, by contrast, have undergone considerable dynamic evolution. Like comets, KBOs formed beyond the snow line of the solar nebula and are therefore believed to contain a large

* R. M. acknowledges support of the Minerva foundation at Tel Aviv University. Some of the results presented here are part of the Ph. D. thesis of R. M., at the Institute of Planetology, University of Muenster.

proportion of H_2O ice. The question addressed here is which of the two classes of small objects do KBOs resemble in terms of thermal evolution? Are they thermally processed objects, like asteroids, or mostly pristine, as comets are presumed to be ? In fact, since short-period (SP) comets — all or some — are believed to originate from KBOs (cf. Duncan et al. 1988), the question of the thermal evolution of KBOs bears directly on the internal structure of comets.

Both asteroids and comets are believed to have been affected by radioactive heat sources, much as larger bodies of the solar system still are. However, since small bodies cool far more effectively than large ones due to their large surface to volume ratio, only high-power (short-lived) radioactive isotopes may be of importance in this case. The radioactive isotope ^{26}Al (with a decay time $\tau = 1.06 \times 10^6$ yr) was recognized as a potential heat source capable of melting bodies of radii between 100 and 1000 km half a century ago (Urey 1955). Evidence for its existence was supplied by ^{26}Mg enhanced abundances found in Ca-Al inclusions of meteorites (e.g., MacPherson et al. 1995). Further support, from an independent source, was provided by the detection of interstellar 1.809 Mev γ-rays from the decay of ^{26}Al (Diehl et al. 1997). All this evidence points towards an interstellar isotopic ratio $^{26}\mathrm{Al}/^{27}\mathrm{Al} \approx 5 \times 10^{-5}$, implying an initial mass fraction $X_0 \approx 7 \times 10^{-7}$ in dust. Indeed, estimates of the potential role of ^{26}Al in the thermal evolution of asteroids showed that it might be sufficient for melting iron (e.g., Merk at el. 2002). In this paper, we address the outcome of internal heating of icy bodies by the decay of ^{26}Al, starting with simple estimates and proceeding to increasingly more complex models.

The potential effect of radiogenic heating during the early evolution of icy bodies may be roughly estimated based on global energy considerations (cf. Prialnik 1998). If we represent such a body of mass M and radius R by a single internal temperature that changes with time, $T(t)$, the energy balance equation is simply

$$M \frac{du}{dt} = M \tau^{-1} X_0 \mathcal{H} \mathrm{e}^{-t/\tau} - 4\pi R^2 (\sigma T_s^4 - \sigma T_e^4), \qquad (1)$$

where the internal energy per unit mass u is obtained by $u = \int c(T) dT$, $c(T)$ being the heat capacity; $\mathcal{H}$ is the radioactive heat released per unit mass (1.48×10^{13} J/kg). $T_s = T(R)$ is the surface temperature and T_e is the temperature of the environment, or the equilibrium temperature at the heliocentric distance d_H of the body. Now, the difference between T_e and the actual surface temperature $T(R)$ is due to heat conduction into or out of the nucleus; in the lowest approximation, $-K \frac{dT}{dr} \sim K \frac{T}{R}$. Hence

$$c(T) \frac{dT}{dt} = \tau^{-1} X_0 \mathcal{H} \mathrm{e}^{-t/\tau} - \frac{3KT}{R^2 \rho}. \qquad (2)$$

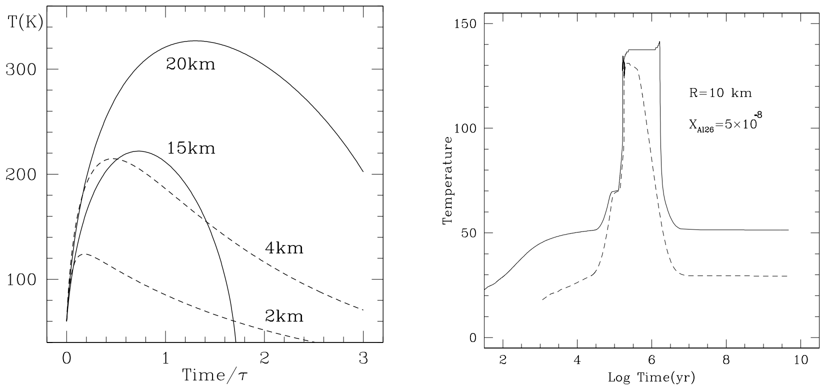

Figure 1. Evolution of temperature as a function of time.*Left*: Analytical solution; parameter values are $T_0 = 60$ K, $X_0 = 7 \times 10{-}8$. Solid lines represent crystalline ice, dashed lines - amorphous ice. *Right*: Numerical solution for maximal internal temperature as a function of time (data from Choi et al. 2002); $d_H = 30$ AU (solid); $d_H = 90$ AU (dashed).

The maximal heating rate, obtained at $t = 0$, is $\tau^{-1}X_0\mathcal{H}$ and for the internal temperature to rise, the RHS of (2) must be positive at $t = 0$, a requirement that is determined by the body's radius and by the thermal conductivity of its material. As the heating rate declines with time, it eventually becomes lower than the rate of cooling in all cases. In conclusion, for suitably large comets the internal temperature rises at the beginning up to a maximal value T_{max} and then falls off, tending to T_e. With the approximation $c(T) \propto T$ — which is valid for $T \gtrsim 50$ K (Klinger 1980) — eq. (2) may be solved analytically for the evolution of $T(t)$. Using the empiric relation $K/\rho c(T) = \kappa =$ constant for amorphous ice,

$$T(t) \approx \left[\frac{2a}{2b\tau - 1}\mathrm{e}^{-t/\tau} + \left(T_0^2 - \frac{2a}{2b\tau - 1}\right)\mathrm{e}^{-2bt/\tau}\right]^{1/2}, \qquad (3)$$

where a and b are constants, and using another empiric relation, $KT =$ constant, for crystalline ice,

$$T(t) \approx [2a(1 - \mathrm{e}^{-t/\tau}) + T_0^2 - 2ft/\tau]^{1/2}, \qquad (4)$$

where f is a constant. From the solutions (3) or (4) we may obtain $T_{max}(R)$, for given T_0 and X_0. Examples are given in Figure 1, and show that above a certain radius, an icy body made of amorphous ice will start crystalizing ($T \gtrsim 120$ K), and above a still larger radius, melting of ice will eventually occur. The answer to our first question is thus a definite *yes*, but we must keep in mind that it was based on very crude approximations. A far more rigorous treatment will be required in order to answer the next question.

2. To what extent are KBOs affected by early radiogenic heating ?

The pioneering work towards answering this question is that of Whipple & Stefanik (1966), who considered the decay of long-lived radionuclides and found that it would lead to loss of the most volatile species. It was followed by the studies of Wallis (1980) and Irvine et al. (1980), who showed by simple calculations that liquid water could be obtained in the core of comet nuclei. The subject was further pursued by Prialnik et al. (1987), Prialnik & Bar-Nun (1990), Yabushita (1993), Haruyama et al. (1993), Prialnik & Podolak (1995), each study focusing on one of the governing parameters, such as thermal conductivity, ^{26}Al content, or radius. Recently, models including mixtures of volatiles and gas flow through the porous medium have been considered by De Sanctis et al. (2001) and by Choi et al. (2002). An example of the results obtained is given in the right panel of Fig. 1, confirming the general behavior derived analytically.

The detailed numerical solution yields temperature profiles and follows the evolution of temperature-dependent processes and the resulting changes in structure. These are better illustrated in Figure 2, which shows the extent of the thermally processed region, assuming an initial composition of amorphous water ice mixed with CO and CO_2 ices as well as dust. For both radii considered (10 km and 100 km), an outer layer about 1 km deep remains relatively cold at all times and thus preserves the ice in amorphous form. In all cases, however, the CO ice is lost, but this is bound to occur in the Kuiper Belt region even in the absence of ^{26}Al (cf. De Sanctis et al. 2001).

To summarize, it appears that icy bodies may be affected by radiogenic heating to a *large extent*, ranging from loss of volatiles to melting of water ice. Since the extent is determined by the competition between processes that take place in parallel, and since the heat source is as short-lived as the accretion of these bodies, we are naturally led to the following question.

3. Is early thermal evolution affected by accretion ?

Consider an accreting body (planetesimal) of mass $M_p(t)$, following a simple growth law

$$M_p(t) = M_{pmax}\left(1 - e^{-t/\theta}\right), \tag{5}$$

where θ is a time constant for accretion, and the law is such that it goes into saturation for $t \to \infty$ with a limit of M_{pmax}, the body's final mass.

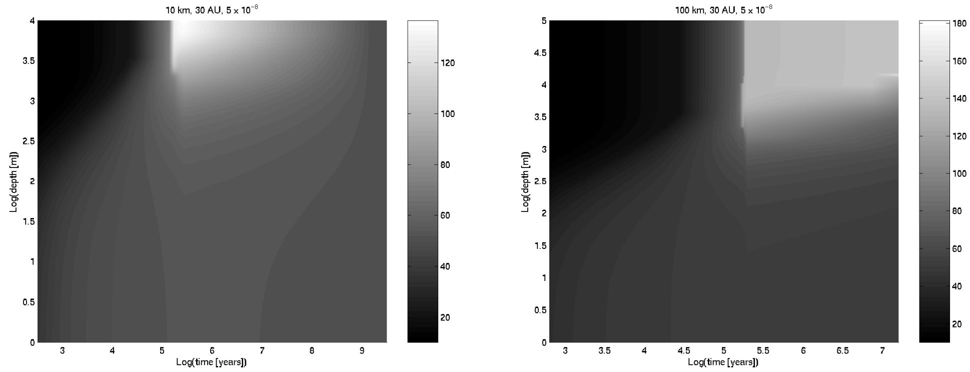

Figure 2. Gray-scale map for the evolving temperature profile (adapted from Choi et al. 2002), for a radius of 10 km (*left*) and 100 km (*right*). The change in color along a vertical line represents the radial temperature variation at the corresponding time. The change in color along a horizontal line represents the change of temperature with time at the corresponding (fixed) depth. The time and depth scales are logarithmic, since changes are more pronounced during the early stages of evolution, and sharper, generally, towards the surface of the nucleus.

Saturation, here, simulates the depletion of mass in the feeding zone of the accreting body. Although such a law cannot be calculated analytically, it provides a fair approximation to detailed numerical results (Weidenschilling 2000). Assume furthermore that the accreted material contains a mass fraction X of radioactive ^{26}Al,

$$X(t) = X_0 e^{-t/\tau} \tag{6}$$

so that the potential (nuclear) energy of the accreting body is

$$E = X(t)\mathcal{H}M_p(t). \tag{7}$$

The rate of internal heating is therefore

$$\begin{aligned} Q(t,\theta,\tau) &= -\dot{E} \\ &= -\dot{X}(t,\tau)\mathcal{H}M_p(t,\theta) - X(t,\tau)\mathcal{H}\dot{M}_p(t,\theta). \end{aligned} \tag{8}$$

This shall be compared with the energy, P, released by a nonaccreting body of full mass M_{pmax}, which is obviously the first term on the LHS of eq.(8) when $M_p(t,\theta) = M_{pmax}$,

$$P(t,\tau) = \frac{1}{\tau} X_0 \mathcal{H} M_{pmax} e^{-t/\tau}. \tag{9}$$

Substituting (5) and (6) into eq. (8) and rearranging terms, we obtain

$$Q(t,\theta,\tau) = P(t,\tau)\left[1 - e^{-t/\theta}\left(1 + \frac{\tau}{\theta}\right)\right], \tag{10}$$

whence it can be seen, as one would expect, that very rapid (instantaneous) accretion (or $\theta \ll \tau$) just yields $\lim_{\theta\to 0} Q(t,\theta,\tau) = P(t,\tau)$. On the other hand, if accretion is very slow ($\theta \gg \tau$), no heating should be expected, since the radioactive material would have decayed before any appreciable amount of mass accumulates. Indeed, (10) yields for this case $\lim_{\theta\to\infty} Q(t,\theta,\tau) = 0$.

Now, accretion theories predict typical accretion-time constants θ similar to the decay constant τ of ^{26}Al. What, then, is the behavior like between the two extremes just considered ? Internal heating can be expected when $Q > 0$, that is, the RHS of (10) is positive,

$$1 - e^{-t/\theta}\left(1 + \frac{\tau}{\theta}\right) > 0. \tag{11}$$

This can be solved for a time t_1 above which the condition is always fulfilled:

$$t_1(\theta,\tau) = \theta \ln\left(1 + \frac{\tau}{\theta}\right). \tag{12}$$

For $\theta = \tau$, we get $t_1 = \tau \ln 2$ and thus at $t = t_1$, we have from (5) and (6)

$$M_p(t_1) = \tfrac{1}{2} M_{pmax}, \qquad X(t_1) = \tfrac{1}{2} X_0. \tag{13}$$

This means that, although the body has yet to accrete half of its final mass, half the original amount of ^{26}Al is still available. In other words, *effective heating starts well during the accretion process and hence cannot be separated from it thermodynamically.* Furthermore, it is already obvious from (10) that $Q < P$, which is why a diminished X_0 is adopted for compensation, when the processes are treated separately, and a fixed mass is assumed at the onset of radioactive decay (as in the studies mentioned in the previous section). This amounts to a constant correction factor for Q, equivalent to a delay time t_0, that is, $e^{-t_0/\tau}$, whereas according to (10), the correction factor Q/P is very different from a constant. In conclusion, accretion and heating by radioactive decay of short-lived isotopes have to be calculated simultaneously.

4. Combined thermal and accretional evolution of icy bodies

4.1. Thermal evolution with moving boundary condition

For a growing, spherically symmetric body of mass $M_p(t)$ and density ρ_p, composed of H_2O ice and dust with mass fractions X_{ice} and X_d, respectively, we choose the mass $0 \le m \le M_p(t)$ as spatial coordinate.

The local heat balance equation allowing for crystallization of amorphous ice, melting and radiogenic heating due to the decay of ^{26}Al, reads

$$\frac{\partial u}{\partial t} = -\frac{\partial F(m,t)}{\partial m} + X_{ice}\dot{X}_a(m,t)H_{ac} + \frac{1}{\tau}X_d X_0 \mathcal{H}\ e^{-t/\tau} \tag{14}$$

$$F(m,t) = -K(T)\left[4\pi\left(\frac{3m}{4\pi\rho_p}\right)^{\frac{2}{3}}\right]^2 \frac{\partial T}{\partial m}. \tag{15}$$

Melting is included in the expression for the internal energy (cf. Weizman et al. 1997), where X_w represents the liquid fraction of H_2O, and c_w and c_d are the heat capacities of water and dust, respectively,

$$u(T) = X_{ice}\left\{[1 - X_w(T)]u_{ice}(T) + X_w(T)\left[H_w + c_w T\right]\right\} + X_d c_d T \tag{16}$$

$$X_w(T) = \frac{1}{1 + e^{\beta(1-T/T_w)}} \tag{17}$$

If $X_a(m,t)$ is the fraction of H_2O in amorphous form and λ, the crystallization rate (Schmitt et al. 1989),

$$\dot{X}_a + \frac{\dot{M}_p}{M_p}\, X_a = -\lambda X_a. \tag{18}$$

The mass coordinate is dynamically scaled as follows (Merk et al. 2002):

$$\eta(m,t) = \frac{m}{M_p(t)} \tag{19}$$

$$\left(\frac{\partial}{\partial m}\right)_t = \frac{1}{M_p(t)}\left(\frac{\partial}{\partial \eta}\right)_t \tag{20}$$

$$\left(\frac{\partial}{\partial t}\right)_m = \left(\frac{\partial}{\partial t}\right)_\eta + \left(\frac{\partial \eta}{\partial t}\right)_m \left(\frac{\partial}{\partial \eta}\right)_t \tag{21}$$

$$= \left(\frac{\partial}{\partial t}\right)_\eta - \frac{\eta}{M_p(t)}\frac{dM_p}{dt}\left(\frac{\partial}{\partial \eta}\right)_t. \tag{22}$$

Finally, the initial and boundary conditions are

$$T(m,0) = T_e(d_H) \tag{23}$$

$$F(0,t) = 0 \tag{24}$$

$$F(M_p(t),t) = 4\pi\left(\frac{3M_p(t)}{4\pi\rho}\right)^{\frac{2}{3}}\left[\epsilon\sigma T^4(M_p(t),t) - \sigma T_e^4(d_H)\right]. \tag{25}$$

4.2. A simple accretion algorithm

For calculating the rate of growth $M_p(t)$ at a given heliocentric distance, we adopt the following procedure. Consider a system of particles of total mass M occupying a volume V, with a discrete mass distribution, so that mass is divided into I intervals between boundaries $b_0 = 0$ and $b_I = M$. Each interval is represented by a mass m_i, satisfying $b_{i-1} < m_i \leq b_i$, say, the mid-point of the interval on a linear or logarithmic scale. Thus, one has a set of fixed masses m_i; $i = 1, ..., I$. If the mass range spans several orders of magnitude, one may define m_i as a geometric series: $m_i = q m_{i-1}$, $q > 1$. Assume further a mass distribution $N_i(m_i)$; $i = 1, ..., I$ and consider binary interactions between particles, such that

$$m_i + m_j \longrightarrow m_k, \tag{26}$$

where k is defined by $b_{k-1} < m_i + m_j \leq b_k$. The mass intervals are defined so that any interaction results in a mass that necessarily belongs to the mass set. In particular, the entire system may coagulate into one particle that still belongs to the system.

If N_i^0; $i = 1, ..., J \leq I$ is the initial distribution, then

$$M = \sum_{i=1}^{J} N_i^0 m_i. \tag{27}$$

How does the mass distribution (or spectrum) evolve with time under the influence of mutual collisions? The number density of particles in the ith bin (of mass m_i) may change due to collisions that destroy or produce such particles, thereby decreasing or increasing their number, respectively. The rate of change of $N_i(t)$ is given by

$$\dot{N}_i = - \sum_j (1 + \delta_{ij}) \frac{A_{ij \to k}}{V} \frac{N_i N_j}{1 + \delta_{ij}} + \sum_{l, k \geq l} \frac{A_{lk \to i}}{V} \frac{N_l N_k}{1 + \delta_{lk}}, \tag{28}$$

with $A_{ij \to k}$ denoting interaction rates (volume per unit time), where indices i and j are independent, while $k = k(i, j)$ as explained above. This is a typical set of *coagulation equations*, or *rate equations* with source and sink terms. The factor $(1 + \delta_{ij})$ in the denominator is due to the collision probability $\frac{1}{2} N^2$ in a system of identical particles. The destruction term under the first sum is multiplied by 2 when $j = i$ because two particles of type i are destroyed in the process.

The interaction rate between particles of types i and j is given by

$$A_{ij \to k} = \pi (r_i + r_j)^2 v_{i,j} (1 + 2\theta_{i,j}), \tag{29}$$

where r_i is the radius of a sphere of mass m_i and material density ρ_p,

$$r_i = \left(\frac{3m_i}{4\pi\rho_p}\right)^{1/3}, \tag{30}$$

and $v_{i,j}$ is the relative velocity of the particles,

$$v_{i,j} = (v_i^2 + v_j^2)^{1/2}. \tag{31}$$

The geometrical cross-section is enhanced by the Safronov parameter $\theta_{i,j}$, given by (Greenzweig & Lissauer 1990, Wetherill & Stewart 1989)

$$\theta_{i,j} = \frac{G(m_i + m_j)}{(r_i + r_j)v_{i,j}^2}. \tag{32}$$

As a very crude approximation, equipartition of kinetic energy is assumed and particle velocities are estimated using the virial theorem (Chandrasekhar 1960):

$$\frac{m_i v_i^2}{2} = \frac{1}{2}\frac{GM^2}{V^{1/3}N}, \tag{33}$$

where N is the total number of particles in the system at a given time, $N = \sum_i N_i(t)$. This approximation proves to be reasonable, as it yields results which are quite similar to those of elaborate velocity calculations (cf. Wetherill & Stewart 1993, Kenyon & Luu 1998).

Since m_i is, in fact, determined only within the accuracy of a mass interval, the equations are transformed to the variable M_i, the total mass in the ith bin, defined by

$$M_i = N_i m_i, \tag{34}$$

Thus, fractional N_i, which (normalized) is regarded as a (smooth) probability rather than an actual number of particles, is allowed. In the new variables, eq.(28) becomes

$$\frac{\dot{M}_i}{m_i} = -\sum_j \frac{A_{ij\to k}}{V}\frac{M_i M_j}{m_i m_j} + \sum_{l,k\geq l}\frac{A_{lk\to i}}{V}\frac{M_l M_k}{(1+\delta_{lk})m_l m_k}, \tag{35}$$

The set of difference equation corresponding to (35) was solved numerically by an implicit method. Finally, the average growth rate that enters the thermal evolution scheme was calculated from

$$M_p(t) = \frac{\sum_{i=1}^{I} N_i(t) m_i}{\sum_{i=1}^{I} N_i(t)} = \frac{M}{N(t)}. \tag{36}$$

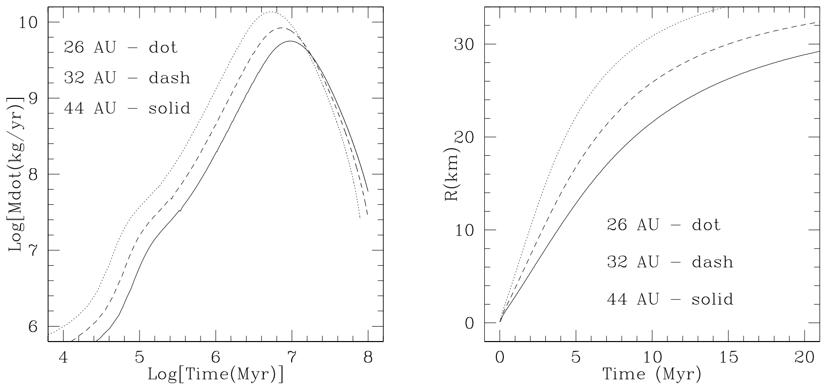

Figure 3. Accretion rate (left) and radius (radius) as a function of time.

The free parameters of this procedure are M and V, or M and the corresponding particle density M/V. This density, like the ambient temperature T_e, is function of the heliocentric distance. We used the model of Bell et al. (1997) for obtaining compatible pairs $[T_e(d_H), \rho(d_H)]$ for our study. There remains a single free parameter M, which was gauged to fit results of the more detailed and extensive calculation of Weidenschilling (2000). [Remarkably, the adjustment of this single parameter, and adoption of the appropriate $\rho(d_H)$, reproduced Weidenschilling's results for planetesimal accretion in the asteroid belt zone.] Examples of the growth rate $\dot{M}_p(t)$ and the corresponding $R_p(t)$ are given in Figure 3.

5. Modeling thermal evolution of growing KBOs

Using the rates of growth supplied by the accretion algorithm, an extensive parameter-space survey was carried out (Merk 2003) for the (d_H, R_{pmax})-plane, spanned by heliocentric distance and maximal radius of the accreting object in the outer region of the Solar System: 2 km$\leq$ R_{pmax} $\leq$32 km and 20 AU$\leq$ d_H $\leq$44 AU. In addition, three different compositions were considered for the homogeneously growing body: ice-rich ($X_{ice} = 0.9$), ice-poor ($X_{ice} = 0.225$), and ice and dust in similar mass fractions ($X_{ice} = 0.45$). Full details of the parameter study will be given elsewhere. In what follows we focus on the intermediate case ($X_{ice}/X_d \approx 1$, characteristic of comets, but not necessarily of KBOs) and refer to the extreme cases only in order to establish trends of behavior. Although the full evolutionary course was followed in each case, we shall focus here on overall results and lasting effects. Within the parameter space, we consider the peak temperatures obtained at the

Table I. Material properties used in models

Property	Value	Units
ρ_d	3500	kg m^{-3}
ρ_{ice}	900	kg m^{-3}
p	0.5	
ρ_p	$(1-p)/(X_{ice}/\rho_{ice}+X_d/\rho_d)$	
H_{ac}	9×10^4	J kg^{-1}
H_w	3.34×10^5	J kg^{-1}
$\mathcal{H}$	1.48×10^{13}	J kg^{-1}
c_a, c_c	$7.49T+90$	J kg^{-1} K^{-1}
c_d	770	J kg^{-1} K^{-1}
c_w	4186	J kg^{-1} K^{-1}
K_a	$2.11\times10^{-3}T+2.5\times10^{-2}$	J kg^{-1}
K_c	$567/T$	J kg^{-1}
K_d	0.1	W m^{-1} K^{-1}
K_w	0.55	W m^{-1} K^{-1}
λ	$1.05\times10^{13}\mathrm{e}^{-5370/T}$	s^{-1}
τ	3.345×10^{13}	s
$\tilde{\beta}$	40	
X_0	6.7×10^{-7}	

center of the body over the (d_H, R_{pmax})-plane, the amount of crystalline ice and the extent of liquid-water zones. Numerical results are presented in the form of *contour plots.* The material parameters used in these calculations (from Klinger 1980, Schmitt et al. 1989, Haak et al. 1990, Alexiades & Solomon 1993, Bennett & McSween 1996) are listed in Table I.

5.1. Temperatures

Figure 4-*top* shows, for $X_{ice} = 0.45$, the peak central temperatures for accreting bodies within the parameter space of final radius and heliocentric distance. A higher dust fraction results in higher temperatures throughout. Above about $X_{ice} = 0.45$, liquid water may be obtained. The temperatures range between 140 K (for $X_{ice} = 0.45$ and the small radii of the parameter space) and more than 350 K.

For a fixed composition at a given heliocentric distance all bodies reach a given radius at the same time. At some point, the accretion time exceeds the life time of ^{26}Al. During the early stage of accretion, the input of energy generated by active ^{26}Al is dominating all other effects, leading to an efficient heating of the bodies' interior. After a while, decaying ^{26}Al can still be compensated by newly accreted active material and the buffering effect of the accreted layers. Accretion provides new active material and, at the same time, serves to insulate the interior. This situation involves the competitive trends of decaying ^{26}Al, substituted radiating material and growing size (which accounts for heat storage). Eventually, the decay of ^{26}Al cannot be compensated anymore and heating ceases. But until this point is reached, heating of the interior proceeds regardless of the final radius. Only after this point, the evolution path of temperatures at $r = 0$ forks due to the evolving radius. This argument holds for a given heliocentric distance (i.e. accretion law) and different radii. It explains the horizontal course of the contours.

5.2. Crystallization

The ice is assumed to be initially amorphous; upon heating, it crystallizes. The fractions of crystalline ice obtained when the crystallization process initiated by the decay of ^{26}Al is completed, are shown in Fig. 4-*middle*. These fractions, ranging between 0 and 1 correspond to R_{ca}/R_{pmax}, where R_{ca} is the radius up to which the ice has crystallized, or the crystalline/amorphous ice boundary. An obvious feature visible in the plot is that the contours follow a maximum at given heliocentric distance. The peak can be found in regions of the parameter space where the corresponding contours of the peak temperature at $r = 0$ become horizontal (cf. Fig. 4-*top*). The left side of the peak can be explained as a consequence of the small size of the accreting bodies and their inability to reach temperatures high enough to cause crystallization of extended regions. The accretion times and the duration of the crystallization process are similar. Close to the region where the peak of the crystalline-ice fraction is obtained, i.e. around 12 km radius for $X_{ice} = 0.45$, the crystallization and accretion fronts move at about the same speed (or one of them is a constant fraction of the other). Therefore, if accretion is terminated for different bodies within this region, their interior crystalline-ice fraction is about the same. Eventually, the crystallization front lags behind the accretion front if the final radius (R_{pmax}) in the parameter space is further increased. The effect results from ceasing energy input due to progressive decay of ^{26}Al: again, accretion outlives radiogenic heating. This results in a declining fraction of crystalline ice and explains the passing of a peak in the parameter plane.

Varying the ice content leads to the following, general result: the fraction of crystalline ice normalized to the radius of the accreted body

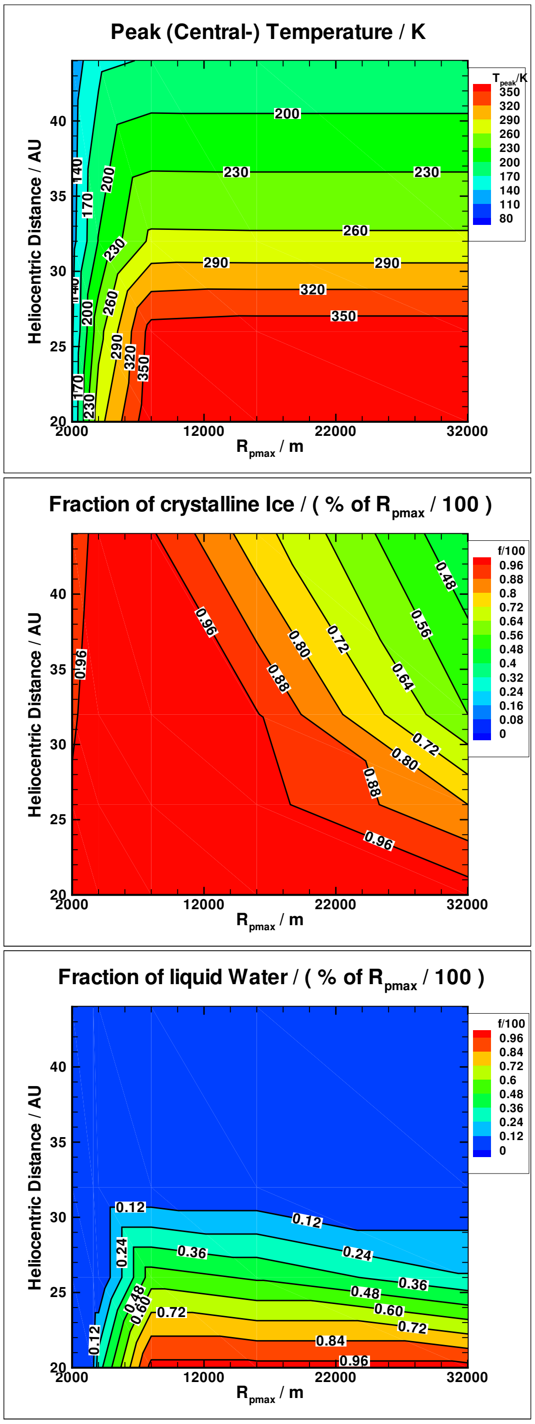

Figure 4. *Top*: Peak temperatures; *Middle*: Fraction of crystalline ice; *Bottom*: Extent of liquid water; for $X_{ice} = 0.45$.

has a maximum in the parameter space between 2 and 12 km regardless of composition and location in the the outer accretion disk. Only for $X_{ice} = 0.9$, pristine (with respect to amorphous ice) 2 km- bodies can be found throughout. For any reduced ice content, processed bodies are found all over the parameter space. Closer to the sun, around 20 AU and less, the ice is crystalline to a large extent. The outmost located and largest bodies, however, show a reduced fraction of interior crystalline ice. This trend is even enhanced by a larger dust content (therefore enhanced heating), since here, slower accretion cannot be overcome by an enhanced ^{26}Al fraction. Finally, the amorphous to crystalline ice transition can be located as a sharp geometric zoning at 100 K.

5.3. Liquid Water

Fig. 4-*bottom* shows the maximum amount of *liquid water* (in terms of relative radius, i.e. extent of the liquid-water zone in the interior, normalized to the maximum radius upon completion of accretion) to be expected in heated and simultaneously accreting icy planetesimals. As before, the results are shown as contours over the parameter space of final radius and heliocentric distance. It is evident that any results related to liquid water inside planetary bodies are significant contributions to the research in this field (e.g., the question of possible bio-organic activity inside these bodies, or the various space missions to comets, present and future).

The figure shows a limited existence of liquid water in areas of the parameter space for $X_{ice} = 0.45$ (i.e., ice/dust ratio $\sim$1). For $X_{ice} = 0.9$, no liquid water whatsoever was obtained. Thus Neptune's present-day orbit (30 AU) seems to describe a borderline. Beyond this heliocentric distance, the fraction of liquid water tends to zero regardless of R_{pmax}. For heliocentric distances smaller than about 30 AU, melting is still not found for the 2 km bodies, even if located as close to the sun (and hence quickly accreting) as 20 AU; these bodies remain permanently frozen. In the intermediate region, melt fractions between 10% to $\sim$ 90% are possible.

In principle, the same argumentation as for the contours relating to crystalline ice (Fig. 4-*middle*) holds here to explain an apparent maximum in the contours at moderate radii. This maximum, however, is less pronounced than in the former case, i.e. the absolute value of the contours' (negative) slope is much smaller. To understand this, one has to consider that the color bands in Fig. 4-*bottom* are much more compressed, that is: the gradient is steeper than in Fig. 4-*middle*. The steep gradient in the d_H-direction is due to the fact that peak temperatures decline to values well below the melting point over half the range of the covered heliocentric distances, i.e. the whole process has 'less room' in the parameter space. The reason is the large difference, about 170 K, between the melting temperature and the temperature range of the transition to crystalline ice. Also, the two processes are different energetically. Crystallization of ice is an exoergic transition, whereas melting of ice is endoergic. Thus, a much smaller slope is sufficient here in order to cause a maximum-like structure within the color bands.

To summarize, one valuable outcome of these calculations is that, for the first time, the region in the early solar system has been determined, where the role of ^{26}Al becomes critical in the sense that it does *not allow* the preservation of pristine ice, although ice should have been able to survive in the nebula in that region, which is much farther out than the snow line. We may call this transition region the *water line*.

6. Conclusions – KBOs as a thermally processed population

We have shown, first by analytical arguments, then by increasingly sophisticated models, that small icy bodies growing in the outer part of the solar nebula, far beyond the snow line, may undergo significant changes due to internal heating by the decay of short-lived radioactive isotopes, in particular ^{26}Al. We have demonstrated that ^{26}Al can be so powerful that the *early* metamorphism of the interior determines the entire evolution, although accretion may continue after its decay.

The critical parameters for the early evolution of KBOs are:

- *Formation distance.* In evolutionary studies that assume a fixed mass and account for the accretion phase by a diminished amount of radioactives (cf. Section 2) the heliocentric distance affects the thermal history of KBOs through the boundary condition (25) and is found to be of only secondary importance (e. g., Choi et al. 2002). When accretion is taken into account simultaneously, the heliocentric distance affects the accretion rate and becomes a crucial factor (as shown in Section 5), even within the restricted range between $\sim$ 25 and $\sim$ 45 AU. This may account for the diversity of structure for objects in this zone, which could not be otherwise understood. It may also imply that comets originating from KBOs should be, on the whole, more pristine than those coming from the Oort cloud, which formed closer to the sun.

- *Final radius.* When bodies of fixed radius are compared in terms of thermal evolution, it is natural to expect higher internal temperatures for larger radii (cf. Section 1). The largest objects would thus be the most processed ones, and the smallest the most pristine.

When growth is considered along with radioactive heating, while it still remains true that the very small objects remain almost unaffected, the largest ones are found to be largely unaffected as well. This is due to the decrease in accretion rate, which causes the outer layers to accumulate very slowly, more slowly than radioactive decay. Thus, there is a range of intermediate radii, where bodies should be expected to be altered the most by radioactivity.

- *Ice/dust ratio.* The ice/dust mass ratio is also the ratio of ice to radioactives content and thus constitutes a key parameter. In an indirect way it affects the results by determining the density of the body (for an assumed porosity), which, in turn, affects the accretion rate (cf. Section 3). For the same d_H and R_{pmax}, we may find, for example, considerable melting of ice or no melting at all, for ice-poor or ice-rich compositions, respectively.

Making allowance for the simplifying assumptions inherent in all models, and for the approximations, and uncertain parameters adopted in the models mentioned here, we can summarize the main results as follows:

- Large KBOs retain the *largest* mass fraction of amorphous ice.
- Liquid water:
  - Ice-poor KBOs: distant ones preserve liquid water longer.
  - Ice-rich KBOs: $R_{pmax} > 15$ km, $d_H \sim 25$ AU, preserve liquid water longest.
  - Dust-poor KBOs - no liquid water.
- It seems possible to have within one object a liquid interior and amorphous ice preserved in the outer part (see Fig. 4).
- Highly volatile species will probably be lost, if they are initially included as ices. The interior may become depleted of less volatile species as well. These however, may be transported to the outer layers, where they can refreeze.
- Large objects are relatively *less* affected than small ones. Very small objects are unaffected at all.

To conclude, it seems highly probable that the population of KBOs is largely — but not entirely — a thermally processed one.

References

Alexiades V., and Solomon A. D., 1993, Mathematical modeling of melting and freezing processes, Hemisphere Publ., Washington.

Bell K. R., Cassen P. M., Klahr H. H., Henning Th., 1997, ApJ, 486, 372.

Bennett M. E., and McSween H. Y., 1996, Meteor. Planet. Sci., 31, 783.

Chandrasekhar S., 1960, The principles of stellar dynamics, Dover, New York.

Choi Y.-J., Cohen M., Merk R., and Prialnik D., 2002, Icarus, 160, 300.

De Sanctis M. C., Capria M. T., and Coradini A., 2001, Astron. J., 121, 2792.

Diehl R., Oberlack U., Knodlseder J., Bloemen H., Hermsen W., Morris D., Ryan J., Schonfelder V., Strong A., von Ballmoos P., Winkler C., 1997, AIP Conference Proceedings 410 (eds. C. D. Dermer, M. S. Strickman, and J. D. Kurfess), p.1114.

Duncan M., Quinn T., and Tremaine S., 1988, Astrophys. J., 328, L69.

Greenzweig Y., and Lissauer J. J., 1990, Icarus, 87, 40.

Haack H., Rasmussen K. L., and Warren P. H., 1990, J. Geophys. Res., 95 B4, 5111.

Haruyama J., Yamamoto T., Mizutani H., and Greenberg J. M., 1993, J. Geophys. Res., 98, 15079.

Irvine W. M., Leschine S., B. and Schloerb F.P., 1980, Nature, 283, 748.

Kenyon S. J., and Luu J. X., 1998, Astron. J., 115, 2136.

Klinger J., 1980, Science, 209, 271.

MacPherson G. J., Davis A. M., and Zinner E. K., 1995, Meteoritics, 30, 365.

Merk R., 2003, Ph.D. thesis.

Merk R., Breuer D., and Spohn T., 2002, Icarus, 159, 183.

Prialnik D., 1998, in Minor Bodies in the Outer Solar system (eds. A. Fitzsimmons, D. Jewitt, and R. M. West), p.33.

Prialnik D., and Bar-Nun A., 1990, Astrophys. J., 355, 281.

Prialnik D., Bar-Nun A., and Podolak M., 1987, Astrophys. J., 319, 992.

Prialnik D., and Podolak M., 1995, Icarus, 117, 420.

Prialnik D., and Podolak M., 1999, Space Sci. Rev., 90, 169.

Schmitt B., Espinasse S., Grim R.J.A., Greenberg J.M., & Klinger J., 1989, ESA-SP,302, 65.

Urey H. C., 1955, Proc. Nat. Acad. Sci., 41, 127.

Wallis M. K., 1980, Nature, 284, 431.

Weidenschilling S. J., 2000, Lunar Planet. Sci. Conf. XXXI, 1684.

Weizman A., Prialnik D., and Podolak M., 1997, J. Geophys. Res., 102, 9205.

Wetherill G. W., and Stewart G. R., 1989, Icarus, 77, 330.

Wetherill G. W., and Stewart G. R., 1993, Icarus, 106, 190.

Whipple F. L., and Stefanik R. P., 1966, Mem. Roy. Soc. Liege (Ser.5), 12, 33.

Yabushita S., 1993, Mon. Not. R. Astron. Soc., 260, 819.

Address for Offprints: Kluwer Prepress Department
P.O. Box 990
3300 AZ Dordrecht
The Netherlands